Volume 4
Number 13
7 July 2022
Pages 2765–2952

Nanoscale Advances

rsc.li/nanoscale-advances

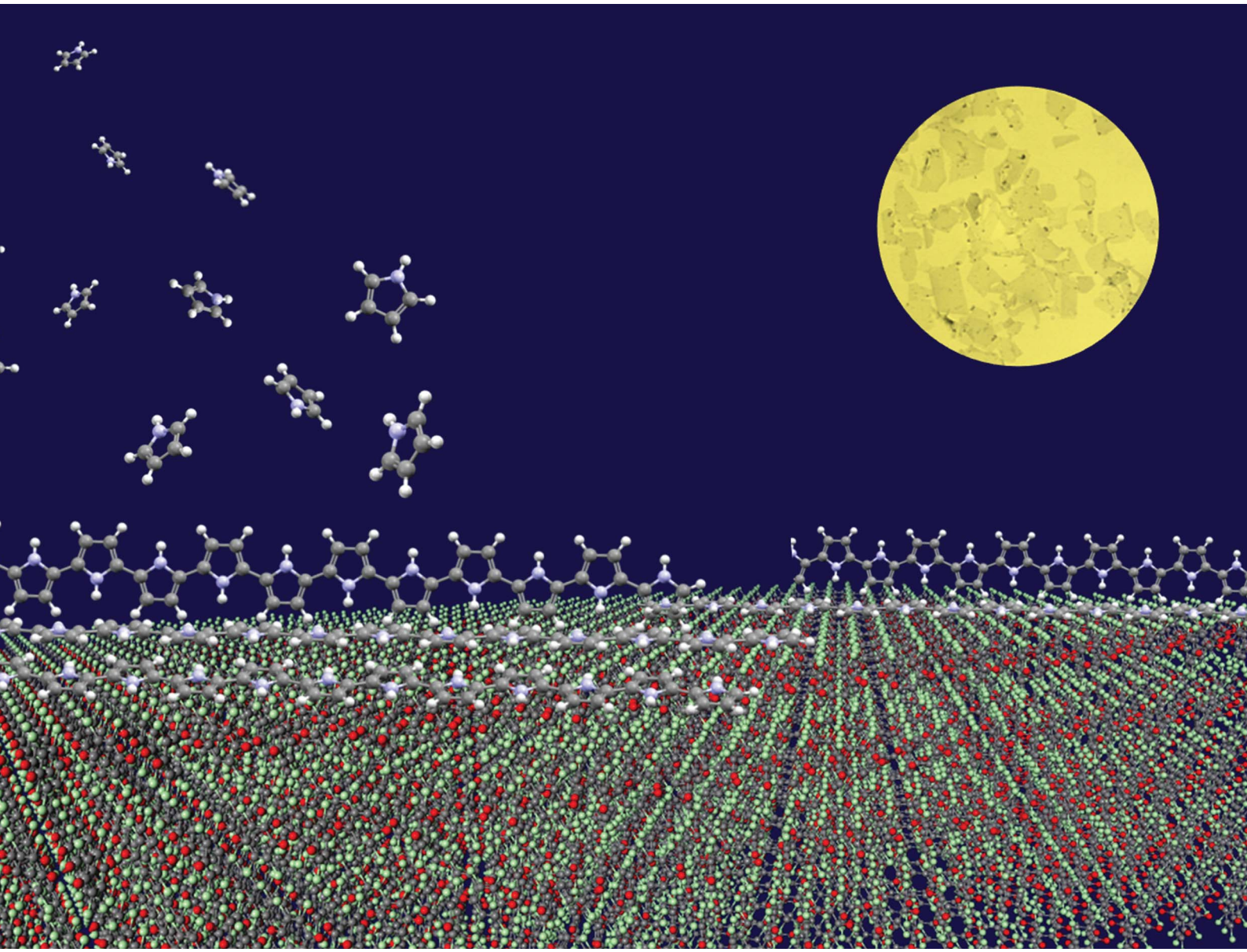

ISSN 2516-0230

ROYAL SOCIETY OF CHEMISTRY

MINIREVIEW
Yuya Oaki and Kosuke Sato
Nanoarchitectonics for conductive polymers using solid and vapor phases

NCNST

Nanoscale Advances

ROYAL SOCIETY OF CHEMISTRY

MINIREVIEW

View Article Online
View Journal | View Issue

Cite this: *Nanoscale Adv.*, 2022, **4**, 2773

Nanoarchitectonics for conductive polymers using solid and vapor phases

Yuya Oaki *[a] and Kosuke Sato [ab]

Conductive polymers have been extensively studied as functional organic materials due to their broad range of applications. Conductive polymers, such as polypyrrole, polythiophene, and their derivatives, are typically obtained as coatings and precipitates in the solution phase. Nanoarchitectonics for conductive polymers requires new methods including syntheses and morphology control. For example, nanoarchitectonics is achieved by liquid-phase syntheses with the assistance of templates, such as macromolecules and porous materials. This minireview summarizes the other new synthetic methods using the solid and vapor phases for nanoarchitectonics. In general, the monomers and related species are supplied from the solution phase. Our group has studied polymerization of heteroaromatic monomers using the solid and vapor phases. The surface and inside of solid crystals were used for the polymerization with the diffusion of the heteroaromatic monomer vapor. Our nanoarchitectonics affords to form homogeneous coatings, hierarchical structures, composites, and copolymers for energy-related applications. The concepts using solid and vapor phases can be applied to nanoarchitectonics for not only conductive polymers but also other polymers toward a variety of applications.

Received 1st April 2022
Accepted 21st April 2022

DOI: 10.1039/d2na00203e

rsc.li/nanoscale-advances

1. Introduction

Nanoarchitectonics is a recent general concept beyond nanotechnology for creation of functional material systems based on nanoscale units.[1] New methods for controlled syntheses and assemblies of the target molecules and materials contribute to advances in nanoarchitectonics.[2] Our group has focused on nanoarchitectonics of functional organic and organic–inorganic composite materials alternative to conventional

[a]*Department of Applied Chemistry, Faculty of Science and Technology, Keio University, 3-14-1 Hiyoshi, Kohoku-ku, Yokohama 223-8522, Japan. E-mail: oakiyuya@applc.keio.ac.jp*

[b]*Organic Materials Chemistry Group, Sagami Chemical Research Institute, 2743-1 Hayakawa, Ayase, Kanagawa 252-1193, Japan*

Yuya Oaki is an Associate Professor of the Department of Applied Chemistry, Keio University, Japan. He received his Ph. D. in 2006 from Keio University and worked at the University of Tokyo as a postdoctoral fellow. His current research interests are layered materials, nanosheets, and conjugated polymers with 2D anisotropy and their applications, such as batteries, catalysts, and sensors. Machine learning is combined with these experimental study based on small data. His research was highlighted by the Chemical Society of Japan Award For Young Chemists for 2015. He also works as a Japan Science and Technology Agency (JST) PRESTO project researcher from 2016.

Kosuke Sato is a Postdoc Researcher of the Organic Material Chemistry Group in Sagami Chemical Research Institute. He received his PhD in Engineering from Keio University in September 2017 under the direction of Associate Professor Yuya Oaki. He studied about morphology control and electrochemical applications of conductive polymers with a research fellowship for young scientists (DC1) from the Japan Society for the Promotion of Science. His current research interests include organic electrodes for energy related applications, organic semiconductor materials, and materials informatics for effective exploration of functional compounds.

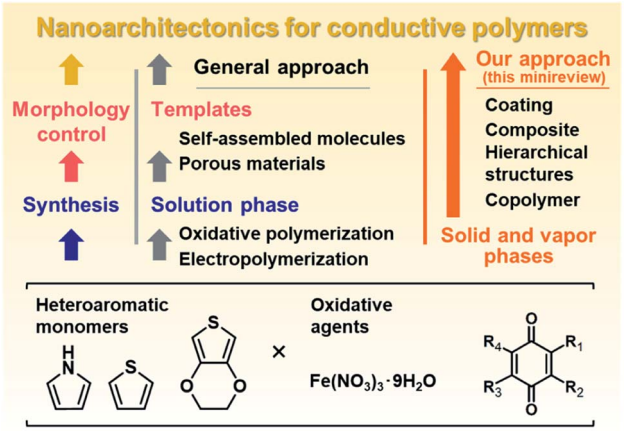

Fig. 1 Schemes of nanoarchitectonics for conductive polymers using the liquid phase by conventional approaches (left) and solid and vapor phases by our methods (right).

molecular design and syntheses.[3–5] In recent years, we have studied nanoarchitectonics for soft two-dimensional (2D) materials, such as layered materials and nanosheets.[3] Soft 2D materials include π-conjugated polymers and layered inorganic–organic composites with flexible structures and dynamic properties.[4,5] Intercalation and exfoliation using the interlayer space are effective methods for nanoarchitectonics of soft 2D materials toward energy and sensing applications.[3] On the other hand, 2D structures are not always formed by typical conductive polymers, such as polythiophene (PTp), polypyrrole (PPy), and polyaniline (PAni). Although the molecular design and synthesis of conductive polymers have been extensively studied, these conductive polymers with the rigid π-conjugated main chain are typically insoluble in solvents. Conductive and conjugated polymers require development of new methods for nanoarchitectonics. Our motivation has been the development of specific methods for the syntheses and morphology control facilitating the nanoarchitectonics, such as formation of coatings, hierarchical structures, and composites, different from typical molecular design and synthesis. This minireview briefly summarizes new nanoarchitectonics for conductive polymers (Fig. 1). Section 2 introduces the liquid-phase syntheses combined with templates as general approaches to nanoarchitectonics (left of Fig. 1). After that, our new nanoarchitectonics using solid and vapor phases are introduced (right of Fig. 1).

2. Conventional nanoarchitectonics for conductive polymers

Conductive polymers show electronic and electrochemical properties originating from the π-conjugated main chain.[6–9] The nanoarchitectonics is significant for a broad range of the applications. Typical synthetic methods are oxidative polymerization and electropolymerization of heteroaromatic monomers (Fig. 1).[6] Oxidation of heteroaromatic monomers, such as pyrrole (Py), thiophene (Tp), and aniline (Ani) derivatives, provides the polymers in the solution phase. In these methods, the reactions and morphologies were controlled by changes in the reaction conditions, such as concentration, temperature, and additive molecules.[10] When the oxidative agent is changed to noble metals, the composite materials of conductive polymers and metal nanoparticles are obtained as precipitates and coatings.[11] However, spontaneous formation of the higher ordered architectures from the nanoscopic to the macroscopic scale is not easily achieved by the polymerization of heteroaromatic monomers in the liquid phase.

Use of templates expands the range of nanoarchitectonics (Fig. 1).[12–16] Self-assembled molecules, such as micelles, assist generation of specific morphologies.[13] Porous materials, such as layered materials, metal–organic frameworks, and mesocrystals, act as the host templates providing a wide variety of morphologies and orientations.[14–16] Morphologies of the templates are replicated in conductive polymers. The solid surface containing the redox-active sites is used for formation of the composites through the surface reaction and coating.[17] For example, coating of conductive polymers on the transition-metal-oxide nanostructures, such as manganese and vanadium oxides, is studied to improve the electrochemical properties for energy storage.[17] The crystal surface of specific materials, such as ice, affords to provide the orientation and crystallinity enabling the enhanced performances, such as conductivity.[18] The nanoarchitectonics using these templates is successfully achieved when the reaction field is confined to the templates with avoiding the polymerization outside of the templates. In this manner, the template-assisted liquid-phase syntheses afford hierarchical morphology replication, reaction control, and diffusion control using the confined space. However, the templates soluble in monomer liquids and solvents are not used for preparation of the composites. Specific methods and optimized conditions are required to ensure the penetration of monomers in the confined space. Nevertheless, the well-established method affords morphology control in a wide range of scales from the nanoscopic to the macroscopic scale, such as conformation and hierarchical forms.

3. Polymerization using solid crystal surfaces

Polymerization using the vapor phase, such as vapor-phase polymerization (VPP) and oxidative-chemical vapor deposition (o-CVD), has been studied for controlled deposition of conductive polymers on a variety of substrates and substances.[19,20] In the VPP method, the matrix polymers, such as poly(vinyl alcohol) and poly(ethylene oxide), containing oxidative agents induce formation of conductive polymers through diffusion of the monomer vapor at low temperature under ambient pressure. The o-CVD method supplies both the monomer and oxidative agent to the target substrates from the vapor phase in a reaction chamber at high temperature under vacuum conditions. The conductive polymers are formed on substrates and substances with the shape conformity. Therefore, the vapor-phase techniques are powerful tools for the

nanoarchitectonics. However, these methods require the pre-coating of the matrix polymer for VPP and specific conditions including low pressure and high temperature for o-CVD. The substrates and substances are limited in these vapor-phase methods.

Our group has studied new polymerization methods for heteroaromatic monomers using the surface and inside of the oxidative agents with diffusion of the monomer vapor at low temperature below 60 °C under ambient pressure.[16a,21–25] In the present paper, the temperature range for syntheses of conductive polymers is defined as room temperature to 100 °C. The melting (T_m) and boiling (T_b) points of typical heteroaromatic monomers are $T_m = -23$ °C and $T_b = 130$ °C for Py and $T_m = 10$ °C and $T_b = 112$ °C for 3,4-ethylenedioxythiophene (EDOT). In addition, organic substrates and substances are stable at temperatures lower than 60 °C. Therefore, the synthetic temperature 60 °C is an appropriate standard for vapor-phase syntheses of conductive polymers on solids in our methods. Section 3 introduces the polymerization of heteroaromatic monomers on the surface of crystals.[21,22] For example, porous morphologies and 2D nanostructures were obtained on the surface of the oxidant crystals with diffusion of the monomer vapor. Section 4 shows the polymerization of heteroaromatic monomers inside of the oxidant crystals with continuous supply of the monomer vapor.[23,24] For example, the redox-active composites of the quinone derivatives and conductive polymers were obtained by the inside polymerization method. The resultant nanoarchitectures are used for energy-related applications,[6a] such as supercapacitors. This minireview summarizes these new nanoarchitectonics for conductive polymers leading to formation of the coating, composite, hierarchical structure, and copolymer (Fig. 1).

3.1 Polymerization on the crystal surface of inorganic and organic oxidants

Section 3 introduces polymerization on the crystal surface of the oxidative agents with diffusion of the heteroaromatic monomer vapor (Fig. 2).[21] Two glass bottles containing heteroaromatic monomers and oxidant crystals were kept in a reaction chamber at 60 °C under ambient pressure (Fig. 2a). The vapor of heteroaromatic monomers, such as AN, Py, EDOT, Tp, and 3-hexylthiophene (HT), is diffused on the surface of solid inorganic oxidant crystals (Fig. 2b).[21a] The oxidation potential of the monomers and reduction potential of the oxidative agents determine whether the conductive polymers are obtained or not (Table 1). As the reaction time increased, the morphologies of the resultant conductive polymers on the surface were changed from the nanoparticles *ca.* 100 nm in size to their accumulated films (Fig. 2c–e).[21a,b] The macroscopic morphology of the oxidant crystal was replicated in the resultant conductive polymers. The micrometer-scale sponge shape of copper sulfate pentahydrate ($CuSO_4 \cdot 5H_2O$) was prepared by freeze drying of the aqueous solution (Fig. 2f). The sponge shape of $CuSO_4 \cdot 5H_2O$ is replicated in PPy (Fig. 2g and h). The resultant PPy sponge consisting of the nanoparticles exhibited a higher specific capacity as a supercapacitor in aqueous electrolyte

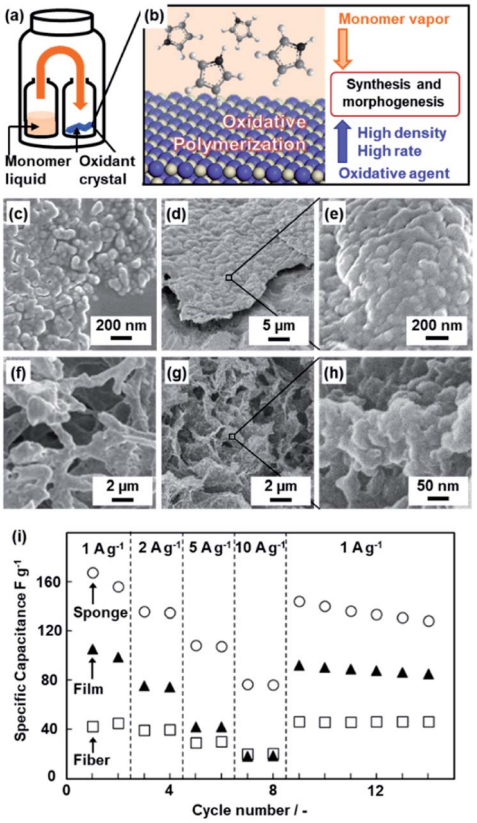

Fig. 2 Polymerization of the heteroaromatic monomer on inorganic oxidant crystals. (a and b) Schematic illustrations of the experimental set up (a) and polymerization reaction on the surface of the oxidant crystals (b). (c–e) Scanning electron microscopy (SEM) images of the PAni nanoparticles after the reaction for 1 h (c) and films consisting of the accumulated nanoparticles after the reaction for 16 h (d and e). (f–h) SEM images of the porous $CuSO_4 \cdot 5H_2O$ crystals by freeze drying (f) and the resultant sponge PPy with the hierarchical structures after polymerization and subsequent dissolution of the inorganic crystals (g and h). (i) Relationship between the current density and specific capacitance of the PPy sponge with the hierarchical structures (circles), films consisting of the nanoparticles (triangles), and commercial fibers (squares). Reproduced from ref. 21*a* with permission from the Royal Society of Chemistry.

Table 1 Combinations of the monomers and oxidant crystals. Reproduced from ref. 21a with permission from the Royal Society of Chemistry

	Monomers				
Oxidant crystals	AN	Py	EDOT	Tp	3HT
$FeCl_3$	+[a]	+	+	+	+
$CuBr_2$	+	+	+	+	–[b]
$CuCl_2 \cdot 2H_2O$	+	+	+	–	–
$Cu(NO_3)_2 \cdot 3H_2O$	+	+	†[c]	–	–
$Cu(CH_3COO)_2 \cdot H_2O$	†	+	–	–	–
$CuSO_4 \cdot 5H_2O$	†	+	–	–	–
$AgNO_3$	+	+	+	–	–

[a] "+" the conductive polymers were obtained. [b] "–" no deposition was observed on the crystal surface. [c] "†" the products were not the polymers.

compared with the film consisting of the nanoparticles and the commercial fibers (Fig. 2i). The high specific surface area originating from the nanoparticles enhances the utilization rate of PPy for the redox reaction with shortening of the diffusion distance. The sponge shape on the micrometer scale ensures the diffusion of the electrolyte.

The oxidative agent was changed to mild organic oxidants, such as quinone derivatives, to improve the conductivity (Fig. 3).[21c,d] Moreover, the reactivity was controlled by the substituents of quinone. The following quinone derivatives with the different oxidation potentials were used for the polymerization (Fig. 3a): 2,3-dichloro-5,6-dicyano-*p*-benzoquinone (DDQ), tetrafluoro-1,4-benzoquinone (TFBQ), tetrachloro-1,4-benzoquinone (TCBQ), tetrabromo-1,4-benzoquinone (TBBQ), 2,5-dichloro-1,4-benzoquinone (DCBQ), 2-chloro-5-methyl-1,4-benzoquinone (CMBQ), and 2,5-dimethyl-1,4-benzoquinone (DMBQ). The reduction potential lowers in this order. The nanosheets were obtained on the surfaces of DDQ, TFBQ, TCBQ, and TBBQ crystals. The thinner nanosheets were obtained with a decrease in the reduction potential at the same reaction time. The PPy nanosheets less than 100 nm in thickness were obtained on the surface of the TBBQ crystal (Fig. 3b and c). On the other hand, the porous sponges were formed on DCBQ and CMBQ because of the higher solubility in the monomer liquid condensed on the surface. In this manner, the reaction and morphology were controlled by the substituents of quinone. The resultant PPy nanosheets exhibited an enhanced conductivity of 287 S cm^{-1} with iodine doping and specific capacitance as an aqueous capacitor (Fig. 3d). This nanoarchitectonics facilitates formation of redox-active and conductive nanosheets with a tunable lateral size and thickness. In this manner, the crystal surfaces as the condensed phase have potential for unique nanoarchitectonics of conductive polymers.

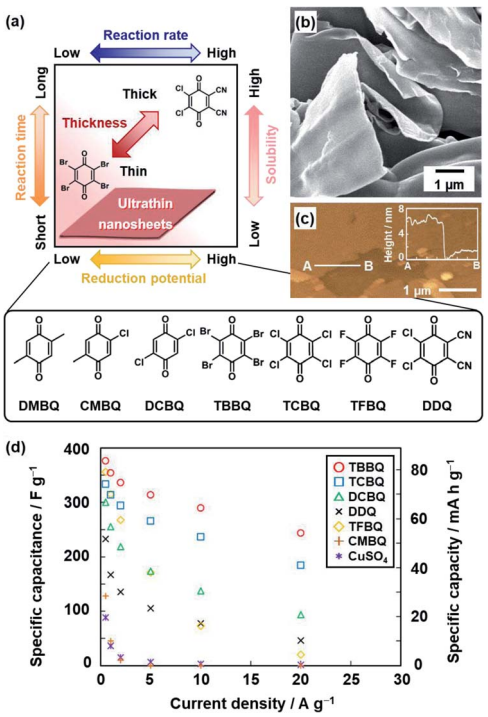

Fig. 3 Polymerization of the heteroaromatic monomer on organic oxidant crystals. (a) Relationship between the reduction potential, reaction time, reaction rate, and thickness. (b and c) SEM and atomic force microscopy (AFM) images with the height profile (inset) of the PPy ultrathin nanosheets formed on TBBQ for 2 h. (d) Relationship between the specific capacity and current density of PPy nanostructures derived from TBBQ (circle), TCBQ (square), DCBQ (triangle), DDQ (cross), TFBQ (diamond), CMBQ (plus), and $CuSO_4$ (asterisk). Reprinted with permission from ref. 21*b*. Copyright 2018 American Chemical Society.

3.2 Activation of heteroaromatic monomers on the crystal surface

Another application of the crystal surface is the generation of activated monomers (Fig. 4).[22] When the heteroaromatic

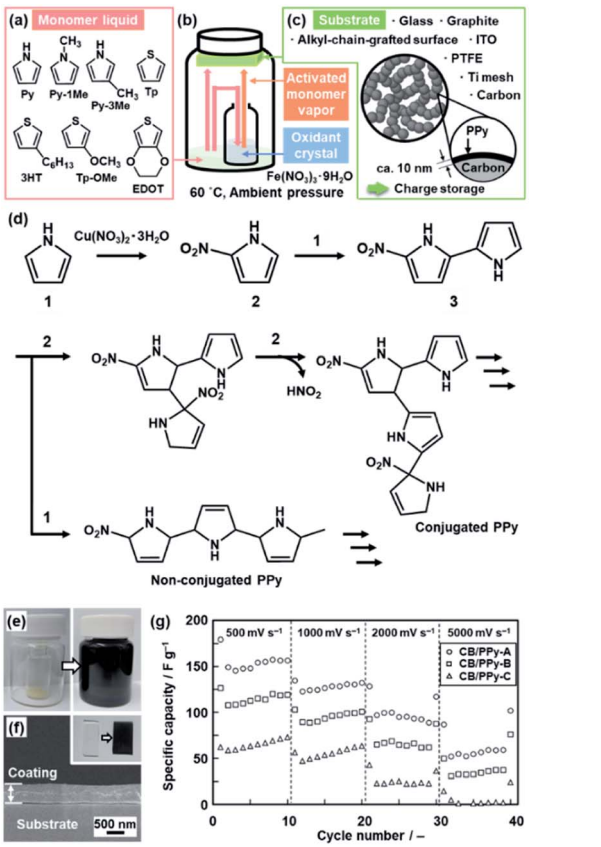

Fig. 4 Polymerization of the heteroaromatic monomer and its activated species on substrates. (a) Molecular structures of the heteroaromatic monomers, such as the pyrrole (Py) and thiophene (Tp) derivatives. (b) Experimental setup for the coating. (c) Substrates for the coating and its application to the energy storage. (d) Synthetic routes of the conjugated and nonconjugated PPy from Py and nitrated Py generated on the surface of the $Cu(NO_3)_2 \cdot 3H_2O$ crystals. (e) Photographs of the sample bottle before (left) and after (right) the coating of PPy. (f) Photograph (the inset) and the cross-sectional SEM image of the PPy coating on a glass substrate for 1 h. (g) Relationship between the scan rate and specific capacity of the samples with the coating time 1 h for CB/PPy-A, 3 h for CB/PPy-B, and 6 h for CB/PPy-C. Reproduced from ref. 22*a* and *b* with permission from the Royal Society of Chemistry.

monomers, such as Py and EDOT, were reacted with transition-metal nitrate crystals and substrates at 60 °C under ambient pressure (Fig. 4a–c), the polymerized products were obtained not only on the surface of the inorganic crystals but also on the surface of the substrates and inner walls of the reaction chamber (Fig. 4e). When original monomers are supplied to the surface of the nitrate crystals, the activated monomers, such as nitrated Py and EDOT, are spontaneously generated at the solid–vapor interface (Fig. 4b and d). The coupling reaction of the original and activated monomers provides the conductive polymers on the surfaces. For example, Py and nitrated Py formed a PPy coating on the substrates in the reaction chamber (Fig. 4e and f). A similar coating was obtained from 1-methylpyrrole (Py-1Me), 3-methylpyrrole (Py-3Me), and 3-methoxythiophene (Tp-3OMe), even though the reaction and coating rates were different. The oxidation potential and evaporation rate of the monomers have effects on the polymerization and coating behavior. Moreover, the thickness was controlled by the coating time.

The coating was used for the energy-related applications. The PPy coating was performed on the surface of lithium titanate ($Li_4Ti_5O_{12}$) nanocrystals *ca.* 100 nm in size as an anode of a lithium-ion battery.[22a] The cycle stability at the higher charge–discharge rate was improved by the PPy-coated $Li_4Ti_5O_{12}$ compared with the bare $Li_4Ti_5O_{12}$ nanocrystals. The surface protection with a conductive coating contributes to the long-term stable charge–discharge reaction. A PPy thin layer of around 10 nm in thickness was coated on carbon black (CB) nanoparticles *ca.* 70 nm in size mounted on titanium (Ti) mesh (Fig. 4c).[22b] The PPy thin layer on the current collector of Ti mesh and CB particles enabled the redox reaction at a high scan rate of 500–5000 mV s^{-1} (Fig. 4g). A redox reaction at such a high scan rate was not observed in previous studies. The ultrathin homogeneous coating on the current collector enhances the utilization rate of PPy for the redox reaction even at the high scan rate.

Two nanoarchitectonics methods for conductive polymers were introduced in this section. The vapor-phase coating using the solid crystal surface affords morphology control and coating of conductive polymers. The crystal surface plays an important role in the reaction and morphology control toward nanoarchitectonics. These approaches can be applied to nanoarchitectonics for other polymer materials.

4. Polymerization using the inside of crystals

4.1 Polymerization in the inside of organic oxidant crystals

Section 4 summarizes polymerization inside the crystals toward nanoarchitectonics.[23,24] The experimental setup is similar to that for polymerization on the crystal surface (Fig. 5). The polymerization inside the crystals provides not only conductive polymers with the controlled morphology but also formation of functional composite materials.[23] The nanocomposites of conductive polymers and redox-active materials were applied to energy storage with enhanced performances.[25] The redox

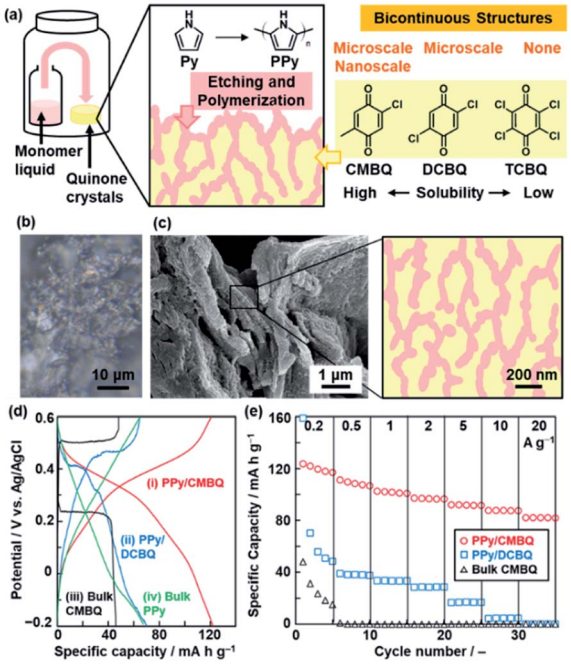

Fig. 5 Polymerization of the heteroaromatic monomer inside of the crystals. (a) Schematic illustration of the experimental setup, etching and polymerization on quinone crystals with diffusion of the monomer vapor, and morphological variation of the composites depending on the quinone derivatives with different solubilities in the monomer. (b) Cross-sectional optical-microscopy image of the pellet consisting of CMBQ crystals after the diffusion of the Py monomer. (c) SEM image and schematic illustration of the PPy/CMBQ microscale bicontinuous structure. (d) Charge–discharge curves of PPy/CMBQ (i, red line), PPy/DCBQ (ii, blue line), and the CMBQ bulk crystal (iii, black line) at 0.2 A g^{-1}. (e) Specific capacity of the PPy/CMBQ composite (red circles), PPy/DCBQ composite (blue squares), and commercial CMBQ bulk crystal (black triangles) at different current densities. Reproduced from ref. 23 with permission from the Royal Society of Chemistry.

reactions of both the components contribute to the specific capacity for the energy storage.[16a,25] Moreover, the conductive polymers in the composite states provide the pathway of the charge carriers to the redox-active materials. However, it is not easy to design and construct such composite structures *via* typical synthetic methods in the solution phase. In our approach, the redox-active quinone derivatives are used as a reactive template for polymerization of Py.[23] The oxidative polymerization of Py was performed in the molded pellet consisting of quinone crystals with a high solubility in Py (Fig. 5a), such as CMBQ.[23] The Py vapor penetrates in the pellet through the grain boundary and then polymerizes in the space between the crystallites and the inside of CMBQ crystals (Fig. 5b and c). The porous PPy/CMBQ composites were obtained on the micrometer scale. Moreover, the bicontinuous nanostructures consisting of the PPy nanoparticles 100 nm in size were formed on the submicrometer scale (Fig. 5c). The composition was estimated to be approximately 40 wt% of PPy and 60 wt% of CMBQ. The hierarchical bicontinuous PPy-CMBQ composite shows enhanced performance as an electrode of a supercapacitor in aqueous media (Fig. 5d and e). The large redox

capacity at high current density originates from the smooth charge transportation to CMBQ through the continuous PPy domain. The PPy network domain also contributes to inhibiting the dissolution of CMBQ in the electrolyte solution. In this manner, the combination of the reactive template and monomer vapor is regarded as a new nanoarchitectonics for generation of composites based on conductive polymers.

4.2 Copolymerization in the inside of organic crystals

In the above cases, solid crystals of quinone derivatives were used as oxidative agents. Herein, the quinone molecule in the solid was embedded in the polymer network through a reaction with Py (Fig. 6).[24] At the interface, benzoquinone (BQ) in the solid phase and Py in the vapor phase induced multistep polymerization reactions including the nucleophilic substitution reaction, Diels–Alder cyclization reaction, and oxidation (Fig. 6a–c). As the pyrrolylene-bridged BQ moieties provide the BQ–Py network polymer through the step-by-step polymerization in the lateral direction, a layered structure is formed due to the graphitic 2D nature of the BQ–Py network (Fig. 6c–f). The layered structure with the loosely stacked BQ–Py network polymers was exfoliated into the nanosheets in dispersion media, such as water and alcohols (Fig. 6d–g). The BQ–Py nanosheets less than 5 nm in thickness were obtained by the exfoliation in the aqueous medium (Fig. 6g). The nanosheets showed enhanced performance as a metal-free electrocatalyst for the hydrogen evolution reaction (HER) (Fig. 6h and i). The overpotential and Tafel slope were lowered after the exfoliation of the BQ–Py layered structure (Fig. 6h and i). The catalytic performance is comparable to that of the other metal-free HER catalysts, such as nanocarbons.[24]

The polymerization reaction was performed in the inside of the crystals. When the solid crystal is an organic oxidant with high solubility in the monomers, formation of conductive polymers proceeds from the interface to the inside through diffusion of the monomer vapor with etching. Moreover, the solid crystal of the reactive comonomers provides the network polymers. These methods using the inside of crystals and the monomer vapor can be regarded as new nanoarchitectonics for conductive polymers.

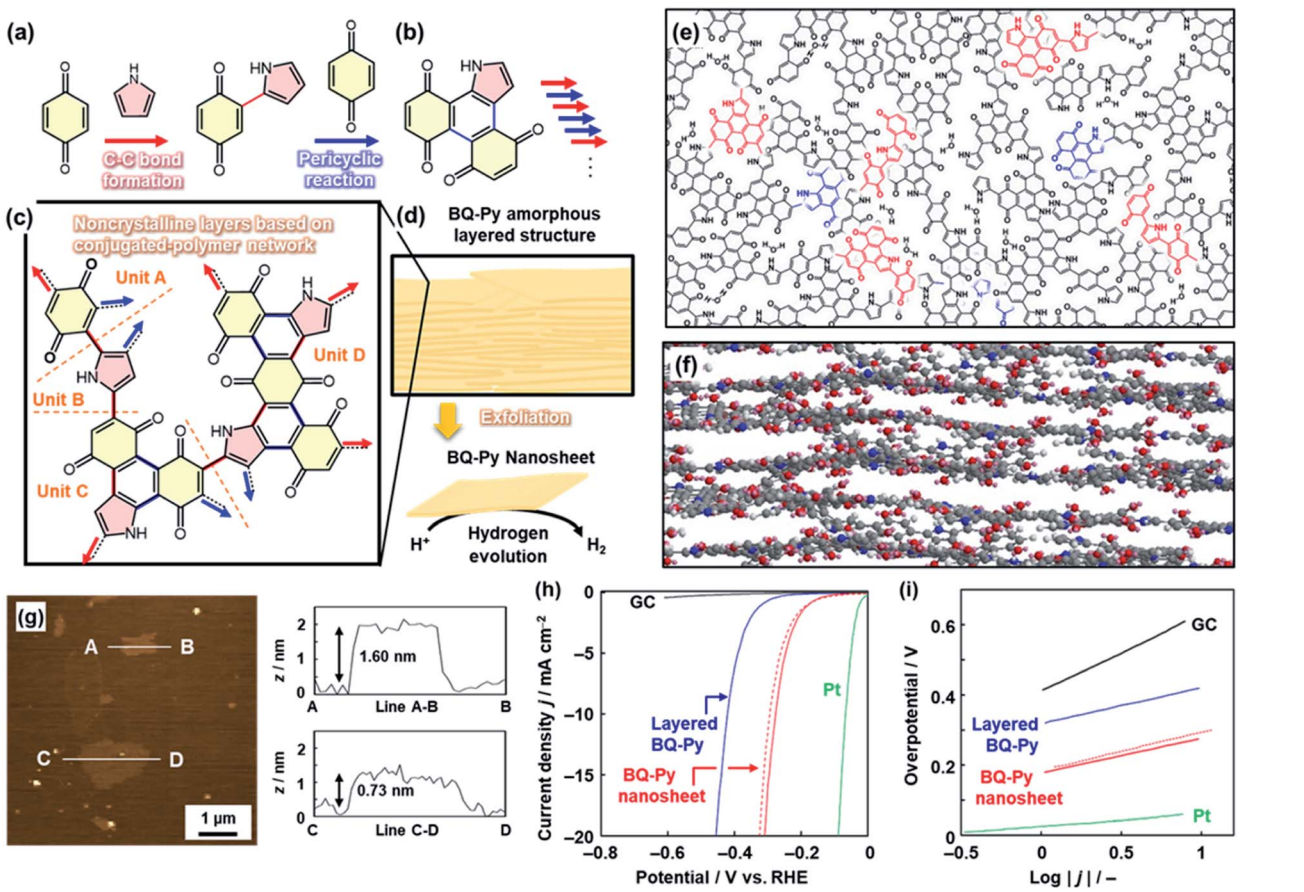

Fig. 6 Copolymerization of the heteroaromatic monomer inside of the crystals. (a and b) Successive C–C bond formation (red arrow) and the pericyclic reaction between BQ and Py (blue arrow). (c) Four structure units of the BQ–Py polymer in the noncrystalline layers. (d) Amorphous layered structure and its exfoliation into the nanosheets with enhanced catalytic properties for the electrochemical HER. (e and f) Schematic models of top (e) and side (f) views of the layered BQ–Py. The upper and lower layers are grown from the red and blue parts in the panel (e), respectively. (g) AFM images and their height profiles. (h and i) LSV curves (h) and Tafel slopes (i) of the bare GC electrode (black line), the layered BQ–Py (blue line), the BQ–Py nanosheets (red line), and the BQ–Py nanosheets after cyclic voltammetry in the range 0 to −0.3 V (*vs.* RHE) for 500 cycles (red dashed line). Reproduced from ref. 24 with permission from the Springer Nature.

5. Summary and outlook

This minireview summarizes recent advances in nanoarchitectonics for conductive polymers. The liquid-phase syntheses combined with templates have been well studied for conventional nanoarchitectonics. On the other hand, we have developed synthetic methods using solid and vapor phases for new nanoarchitectonics. The vapor of heteroaromatic monomers is diffused on the solid surfaces at low temperature under ambient pressure. The homogeneous coatings, hierarchical structures, composites, and copolymers are obtained depending on the solid inorganic and organic crystals. The solid–vapor interface polymerization confines the reaction field on the surface. The reactants can be smoothly supplied at the interface and converted to products without interruption of solvents. The condensed environment at the interface is different from the diluted one in the liquid-phase polymerization. The crystal surface of inorganic and organic oxidants provides the nanoparticle-based forms and flat 2D morphologies depending on the polymerization rate at the nanoscale, respectively. The oxidants with the higher solubility provide the composites with the bicontinuous morphology. Moreover, the macroscopic morphologies larger than the micrometer scale are replicated in the polymers. In this manner, our new nanoarchitectonics can be applied to design hierarchical structures from the nanoscale to the macroscopic scale. Although these concepts and methodologies are now only applied to the limited combinations of heteroaromatic monomers and solid crystals, a variety of nanoarchitectures can be designed and synthesized through different solid–vapor combinations.

These nanoarchitectonics can be used in energy-related applications, such as batteries and capacitors. As a new application of conductive polymers, photothermal conversion properties have attracted much interest to design light-responsive materials.[26] For example, Fujii *et al.* applied conversion of conductive polymers to heteroatom-doped nanocarbons with irradiation of near infrared (NIR) light at room temperature.[27] The fact suggests that nanoarchitectonics for conductive polymers in this minireview can be used for the generation of new functional nanocarbons. Moreover, nanoarchitectonics for conductive polymers requires further advances as a tool for development of functional materials.

Conflicts of interest

There are no conflicts to declare.

Acknowledgements

The authors thank all the collaborators as listed in the literature cited in the reference section. This work was partially supported by a Grant-in-Aid for Scientific Research on Innovative Areas of "Fusion Materials: Creative Development of Materials and Exploration of Their Function through Molecular Control" (No. 2206) from the Ministry of Education, Culture, Sports, Science and Technology, by a Grant-in-Aid for Young Scientists (A, No. 21850025) from the Japan Society for the Promotion of Science, by JST PRESTO (JPMJPR16N2), by the Tonen General Research Foundation, by Sekisui Chemical Nature Research Program (Y. O.), by the Ogasawara Foundation for the Promotion of Science & Engineering, by the Noguchi Institute, and by Toray Science Foundation (20-6103). One of the authors (K. S.) is grateful for a JSPS Research Fellowship for Young Scientists (16J03122).

Notes and references

1 (*a*) K. Ariga, *Nanoscale Horiz*, 2021, **6**, 364; (*b*) K. Ariga and M. Shionoya, *Bull. Chem. Soc. Jpn.*, 2021, **94**, 839; (*c*) J. Liu, H. Zhou, W. Yang and K. Ariga, *Acc. Chem. Res.*, 2020, **53**, 644; (*d*) K. Ariga, T. Mori, T. Kitao and T. Uemura, *Adv. Mater.*, 2020, **32**, 1905657; (*e*) K. Ariga and L. K. Shrestha, *Adv. Intl. Syst.*, 2020, **2**, 1900157; (*f*) X. Liang, L. Li, J. Tang, M. Komiyama and K. Ariga, *Bull. Chem. Soc. Jpn.*, 2020, **93**, 581.

2 (*a*) T. Kato, N. Mizoshita and K. Kishimoto, *Angew. Chem., Int. Ed.*, 2006, **45**, 38; (*b*) T. Aida, E. W. Meijer and S. I. Stupp, *Science*, 2012, **335**, 813; (*c*) T. Kato, J. Uchida, T. Ichikawa and T. Sakamoto, *Angew. Chem., Int. Ed.*, 2018, **57**, 4355; (*d*) X. Xu, K. Müllen and A. Narita, *Bull. Chem. Soc. Jpn.*, 2020, **93**, 490; (*e*) E. A. Neal and T. Nakanishi, *Bull. Chem. Soc. Jpn.*, 2021, **94**, 1769; (*f*) T. Kato, M. Gupta, D. Yamaguchi, K. P. Gan and M. Nakayama, *Bull. Chem. Soc. Jpn.*, 2021, **94**, 357.

3 (*a*) Y. Oaki, *Chem. Commun.*, 2020, **56**, 13069; (*b*) Y. Oaki, *Chem. Lett.*, 2021, **50**, 305; (*c*) Y. Oaki and Y. Igarashi, *Bull. Chem. Soc. Jpn.*, 2021, **94**, 2410.

4 (*a*) Y. Ishijima, H. Imai and Y. Oaki, *Chem*, 2017, **3**, 509; (*b*) H. Terada, H. Imai and Y. Oaki, *Adv. Mater.*, 2018, **30**, 1801121; (*c*) K. Watanabe, H. Imai and Y. Oaki, *Small*, 2020, **16**, 2004586; (*d*) J. Suzuki, A. Ishizone, K. Sato, H. Imai, Y. J. Tseng, C. H. Peng and Y. Oaki, *Chem. Sci.*, 2020, **11**, 7003; (*e*) M. Nakamitsu, K. Oyama, H. Imai, S. Fujii and Y. Oaki, *Adv. Mater.*, 2021, **33**, 2008755.

5 (*a*) G. Nakada, H. Imai and Y. Oaki, *Chem. Commun.*, 2018, **54**, 244; (*b*) R. Mizuguchi, H. Imai and Y. Oaki, *Nanoscale Adv*, 2020, **2**, 1168; (*c*) K. Noda, Y. Igarashi, H. Imai and Y. Oaki, *Adv. Theory Simul.*, 2020, **3**, 2000084; (*d*) R. Mizuguchi, Y. Igarashi, H. Imai and Y. Oaki, *Nanoscale*, 2021, **13**, 3853; (*e*) K. Noda, Y. Igarashi, H. Imai and Y. Oaki, *Chem. Commun.*, 2021, **57**, 5921.

6 (*a*) H. Shirakawa, *Angew. Chem., Int. Ed.*, 2001, **40**, 2574; (*b*) G. Inzelt, *Conducting Polymers - A New Era in Electrochemistry*. Springer. Berlin. 2008; (*c*) J. Roncail, *Macromol. Rapid Commn.*, 2007, **28**, 1761; (*d*) A. Eftekhari, *Nanostructured Conductive Polymers*. Wiley. New York. 2011; (*e*) R. C. Advincula, *J. Am. Chem. Soc.*, 2011, **133**, 5622; (*f*) S. Inagi, *Polym. J.*, 2019, **51**, 975; (*g*) C. I. Idumah, *Syn. Metals*, 2021, **273**, 116674; (*h*) K. Namsheer and C. S. Rout, *RSC Adv.*, 2021, **11**, 5659; (*i*) Y. Yin, S. Chen, S. Zhu, L. Li, D. Zhai, D. Huang and J. Peng, *Macromolecules*, 2021, **54**, 4571; (*j*) J. Peng and Y. Han, *Giant*, 2020, **4**, 100039; (*k*) S. Cheng, R. Zhao and D. S. Seferos, *Acc. Chem. Res.*, 2021, **54**, 4203.

7 (*a*) S. I. Cho and S. B. Lee, *Acc. Chem. Res.*, 2008, **41**, 699; (*b*) G. Snook, P. Kao and A. Best, *J. Power Sources*, 2011, **196**, 112; (*c*) Y. Zhao, B. Liu, L. Pan and G. Yu, *Energy Environ. Sci.*, 2013, **6**, 2856; (*d*) K. Wang, H. Wu, Y. Meng and Z. Wei, *Small*, 2014, **10**, 14; (*e*) Y. Shi, L. Peng, Y. Ding, Y. Zhao and G. Yu, *Chem. Soc. Rev.*, 2015, **44**, 6684; (*f*) A. M. Bryan, L. M. Santino, Y. Lu, S. Acharya and J. M. D'Arcy, *Chem. Mater.*, 2016, **28**, 5989; (*g*) S. Tajik, H. Beitollahi, F. G. Nejad, I. S. Shoaie, M. A. Khalilzadeh, M. S. Asl, Q. V. Le, K. Zhang, H. W. Jang and M. Shokouhimehr, *RSC Adv.*, 2020, **10**, 37834.

8 (*a*) H. Zeng, H. He, Y. Fu, T. Zhao, W. Han, L. Xing, Y. Zhang, Y. Zhan and X. Xue, *Nanoscale*, 2018, **10**, 19987; (*b*) H. Li, G. Gao, Z. Xu, D. Tang and T. Chen, *Macomol. Rapid Commun.*, 2021, **42**, 2100480; (*c*) S. Peng, Y. Yu, S. Wu and C. H. Wang, *ACS Appl. Mater. Interfaces*, 2021, **13**, 43831; (*d*) Y. Gao, D. Liu, Y. Xie, Y. Song, E. Zhu, Z. Shi, Q. Yang and C. Xiong, *J. Appl. Polym. Sci.*, 2021, **138**, 51367; (*e*) C. Du, Y. Zhang, D. Zhang, B. Zhang and W. Zhao, *J. Mater. Chem. C*, 2021, **9**, 13172; (*f*) S. Du, H. Suo, G. Xie, Q. Lyu, M. Mo, Z. Xie, N. Zhou, L. Zhang, J. Tao and J. Zhu, *Nano Energy*, 2022, **93**, 106906.

9 (*a*) S. Nambiar and J. T. W. Yeow, *Biosens. Bioelectron.*, 2011, **26**, 1825; (*b*) L. Li, Y. Shi, L. Pan, Y. Shi and G. Yu, *J. Mater. Chem. B*, 2015, **3**, 2920; (*c*) N. Aydemir, J. Malmström and J. Travas-Sejdic, *Phys. Chem. Chem. Phys.*, 2016, **18**, 8264; (*d*) T. R. Pavase, H. Lin, Q. Shaikh, H. Sameer, Z. Li, I. Ahmed, L. Lv, L. Sun, S. B. H. Shah and M. T. Kalhoro, *Sens. Actuators B Chem.*, 2018, **273**, 1113; (*e*) H. Liu, Q. Li, S. Zhang, R. Yin, X. Liu, Y. He, K. Dai, C. Shan, J. Guo, C. Liu, C. Shen, X. Wang, N. Wang, Z. Wang, R. Wei and Z. Guo, *J. Mater. Chem. C*, 2018, **6**, 12121; (*f*) J. Chen, Q. Yu, X. Cui, M. Dong, J. Zhang, C. Wang, J. Fan, Y. Zhu and Z. Guo, *J. Mater. Chem. C*, 2019, **7**, 11710; (*g*) J. Qin, J. Gao, X. Shi, J. Chang, Y. Dong, S. Zheng, X. Wang, L. Feng and Z. Wu, *Adv. Funct. Mater.*, 2020, **30**, 1909756.

10 (*a*) J. D. Noll, M. A. Nicholson, P. G. V. Patten, C. W. Chung and M. L. Myrick, *J. Electrochem. Soc.*, 1998, **145**, 3320; (*b*) J. Duchet, R. Legras and S. Demoustier-Champagne, *Synth. Met.*, 1998, **98**, 113; (*c*) S. D. Champagne and P.-Y. Stavaux, *Chem. Mater.*, 1999, **11**, 829; (*d*) X. Zhang and S. K. Manohar, *J. Am. Chem. Soc.*, 2004, **126**, 12714; (*e*) X. Yang, T. Dai, Z. Zhu and Y. Lu, *Polymer*, 2007, **48**, 4021; (*f*) J. Zang, C. M. Li, S. J. Bao, X. Cui, Q. Bao and C. Q. Sun, *Macromolecules*, 2008, **41**, 7053; (*g*) S. Carquigny, O. Segut, B. Lakard, F. Lallemand and P. Fievet, *Synth. Met.*, 2008, **158**, 453; (*h*) R. G. Northcutt and V. B. Sundaresan, *J. Mater. Chem. A*, 2014, **2**, 11784; (*i*) A. Fakhry, H. Cachet and C. Debiemme-Chouvy, *Electrochim. Acta*, 2015, **179**, 297; (*j*) A. Xie, F. Wu, W. Jiang, K. Zhang, M. Sun and M. Wang, *J. Mater. Chem. C*, 2017, **5**, 2175; (*k*) K. Ishii, K. Sato, Y. Oaki and H. Imai, *Polym. J.*, 2019, **51**, 11.

11 (*a*) S. Fujii, A. Aichi, K. Akamatsu, H. Nawafune and Y. Nakamura, *J. Mater. Chem.*, 2007, **17**, 3777; (*b*) S. Fujii, S. Matsuzawa, Y. Nakamura, A. Ohtaka, T. Teratani, K. Akamatsu, T. Tsuruoka and H. Nawafune, *Langmuir*, 2010, **26**, 6230; (*c*) S. Fujii, S. Matsuzawa, H. Hamasaki, Y. Nakamura, A. Bouleghlimat and N. J. Buurma, *Langmuir*, 2012, **28**, 2463; (*d*) H. Takeoka, M. Seike, Y. Nakamura, H. Imai, Y. Oaki and S. Fujii, *Mater. Adv.*, 2022, **3**, 931.

12 (*a*) C. Martin, *Acc. Chem. Res.*, 1995, **28**, 61; (*b*) V. M. Cepak and C. R. Martin, *Chem. Mater.*, 1999, **11**, 1363; (*c*) K. Tajima and T. Aida, *Chem. Commun.*, 2000, 2399; (*d*) H. P. Hentze and M. Antonietti, *Curr. Opin. Solid State Mater. Sci.*, 2001, **5**, 343; (*e*) R. A. Caruso and M. Antonietti, *Chem. Mater.*, 2001, **13**, 3272; (*f*) K. J. C. van Bommel, A. Friggeri and S. Shinkai, *Angew. Chem., Int. Ed.*, 2003, **42**, 980; (*g*) S. J. Hurst, E. K. Payne, L. Qin and C. A. Mirkin, *Angew. Chem., Int. Ed.*, 2006, **45**, 2672; (*h*) T. L. Kelly and M. O. Wolf, *Chem. Soc. Rev.*, 2010, **39**, 1526; (*i*) J. Martín, J. Maiz, J. Sacristan and C. Mijangos, *Polymer*, 2012, **53**, 1149; (*j*) X. Y. Yang, L. H. Chen, Y. Li, J. C. Rooke, C. Sanchez and B. L. Su, *Chem. Soc. Rev.*, 2017, **46**, 481; (*k*) S. Mochizuki, T. Kitao and T. Uemura, *Chem. Commun.*, 2018, **54**, 11843; (*l*) N. Hosono and T. Uemura, *Bull. Chem. Soc. Jpn.*, 2021, **94**, 2139.

13 (*a*) V. P. Menon, J. Lei and C. R. Martin, *Chem. Mater.*, 1996, **8**, 2382; (*b*) I. Ichinose, H. Miyauchi, M. Tanaka and T. Kunitake, *Chem. Lett.*, 1998, 19; (*c*) I. Ichinose and T. Kunitake, *Adv. Mater.*, 1999, **11**, 413; (*d*) A. D. W. Carswell, E. A. O'Rea and B. P. Grady, *J. Am. Chem. Soc.*, 2003, **125**, 14793; (*e*) X. Zhang, J. Zhang, Z. Liu and C. Robinson, *Chem. Commun.*, 2004, 1852–1853; (*f*) V. Bocharova, A. Kiriy, H. Vinzelberg, I. Mönch and M. Stamm, *Angew. Chem., Int. Ed.*, 2005, **44**, 6391; (*g*) J. Y. Kim, J. T. Kim, E. A. Song, Y. K. Min and H. Hamaguchi, *Macromolecules*, 2008, **41**, 2886; (*h*) Y. Han, X. Qing, S. Ye and Y. Lu, *Synth. Met.*, 2010, **160**, 1159; (*i*) S. Liu, F. Wang, R. Dong, T. Zhang, J. Zhang, X. Zhuang, Y. Mai and X. Feng, *Adv. Mater.*, 2016, **28**, 8365; (*j*) S. Liu, F. Wang, R. Dong, T. Zhang, J. Zhang, Z. Zheng, Y. Mai and X. Feng, *Small*, 2017, **13**, 1604099.

14 (*a*) Q. Wu, Z. Xue, Z. Qi and F. Wang, *Polymer*, 2000, **41**, 2029; (*b*) D. H. Song, H. M. Lee, K. H. Lee and H. J. Choi, *J. Phys. Chem. Solids*, 2008, **69**, 1383; (*c*) G. Ni, J. Cheng, X. Dai, Z. Guo, X. Ling, T. Yu and Z. Sun, *Electroanalysis*, 2018, **30**, 2366; (*d*) Y. Tong, M. He, Y. Zhou, X. Zhong, L. Fan, T. Huang, Q. Liao and Y. Wang, *Appl. Surface Sci.*, 2018, **434**, 283; (*e*) X. Wang, Y. Ma, X. Sheng, Y. Wang and H. Xu, *Nano Lett.*, 2018, **18**, 2217; (*f*) U. Riaz, N. Singh, A. Verma and E. S. Aazam, *Polym. Eng. Sci.*, 2020, **60**, 2628; (*g*) Z. Feng, J. Sun, Y. Liu, H. Jiang, M. Cui, T. Hu, C. Meng and Y. Zhang, *ACS Appl. Mater. Interfaces*, 2021, **13**, 61154.

15 (*a*) N. Yanai, T. Uemura, M. Ohba, Y. Kadowaki, M. Maesato, M. Takenaka, S. Nishitsuji, H. Hasegawa and S. Kitagawa, *Angew. Chem., Int. Ed.*, 2008, **47**, 9883; (*b*) T. Uemura, N. Uchida, A. Asano, A. Saeki, S. Seki, M. Tsujimoto, S. Isoda and S. Kitagawa, *J. Am. Chem. Soc.*, 2012, **134**, 8360; (*c*) T. Uemura, T. Kaseda, Y. Sasaki, M. Inukai, T. Toriyama, A. Takahara, H. Jinnai and S. Kitagawa, *Nat. Commun.*, 2015, **6**, 7473; (*d*) C. J. Lu, T. Ben, S. X. Xu and S. L. Qiu, *Angew. Chem., Int. Ed.*, 2014, **53**, 6454; (*e*) Y. Jiao, G. Chen, D. Chen, J. Pei and Y. Hu, *J. Mater. Chem. A*,

2017, **5**, 23744; (*f*) Y. Liu, N. Xu, W. Chen, X. Wang, C. Sun and Z. Su, *Dalton Trans.*, 2018, **47**, 13472; (*g*) W. Wang, W. Zhao, T. Chen, Y. Bai, H. Xu, M. Jiang, S. Liu, W. Huang and Q. Zhao, *Adv. Funct. Mater.*, 2021, **31**, 2010306.

16 (*a*) Y. Oaki and K. Sato, *J. Mater. Chem. A*, 2018, **6**, 23197; (*b*) Y. Oaki, M. Kijima and H. Imai, *J. Am. Chem. Soc.*, 2011, **133**, 8594; (*c*) M. Kijima, Y. Oaki, Y. Munekawa and H. Imai, *Chem. -Eur. J.*, 2013, **19**, 2284; (*d*) A. Göppert and H. Cölfen, *RSC Adv.*, 2018, **8**, 33748.

17 (*a*) L. Pan, L. Pu, Y. Shi, S. Song, X. Zhou, R. Zhang and Y. Zheng, *Adv. Mater.*, 2007, **19**, 461; (*b*) J. Zhang, Y. Shi, Y. Ding, W. K. Zhang and G. H. Yu, *Nano Lett.*, 2016, **16**, 7276; (*c*) X. Hong, Y. Liu, Y. Li, X. Wang, J. Fu and X. Wang, *Polymers*, 2020, **12**, 331; (*d*) S. He, X. Sun, H. Zhang, C. Yuan, Y. Wei and J. Li, *Macromol. Rapid Comm.*, 2021, **42**, 2100324; (*e*) Y. Xu, M. Chen, H. Wang, C. Zhou, Q. Ma, Q. Deng, X. Wu and X. Zeng, *Nanoscale*, 2021, **14**, 1008–1013; (*f*) Z. Feng, J. Sun, Y. Liu, H. Jiang, M. Cui, T. Hu, C. Meng and Y. Zhang, *ACS Appl. Mater. Interfaces*, 2021, **13**, 61154.

18 (*a*) S. S. Jeon, H. H. An, C. S. Yoon and S. S. Im, *Polymer*, 2011, **52**, 652; (*b*) I. Y. Choi, J. Lee, H. Ahn, J. Lee, H. C. Choi and M. J. Park, *Angew. Chem., Int. Ed.*, 2015, **54**, 10497; (*c*) K. Kim and M. J. Park, *Nanoscale*, 2020, **12**, 14320; (*d*) K. Kim, B. Kim, K. Kim and M. J. Park, *Macomol. Rapid Commun.*, 2021, **42**, 2100565.

19 (*a*) H. Bai, C. Li, F. Chen and G. Shi, *Polymer*, 2007, **48**, 5259; (*b*) D. Bhattacharyya, R. M. Howden, D. C. Borrelli and K. K. Gleason, *J. Polym. Sci. B Polym. Phys.*, 2012, **50**, 1329; (*c*) A. M. Coclite, R. M. Howden, D. C. Borrelli, C. D. Petruczok, R. Yang, J. L. Yagüe, A. Ugur, N. Chen, S. Lee, W. J. Jo, A. Liu, X. Wang and K. K. Gleason, *Adv. Mater.*, 2013, **25**, 5392; (*d*) R. Brooke, P. Cottis, P. Talemi, M. Fabretto, P. Murphy and D. Evans, *Prog. Mater. Sci.*, 2017, **76**, 127.

20 (*a*) J. P. Lock, S. G. Im and K. K. Gleason, *Macromolecules*, 2006, **39**, 5326; (*b*) M. H. Grarahcheshmeh and K. K. Gleason, *Adv. Mater. Interfaces*, 2019, **6**, 1801564; (*c*) D. Bilger, S. Z. Homayounfar and T. L. Andrew, *J. Mater. Chem. C*, 2019, **7**, 7159.

21 (*a*) K. Kuwabara, Y. Oaki, R. Muramatsu and H. Imai, *Chem. Commun.*, 2015, **51**, 9698; (*b*) Y. Oaki, R. Muramatsu and H. Imai, *Polym. J.*, 2015, **47**, 183; (*c*) K. Sato, H. Imai and Y. Oaki, *ACS Appl. Nano Mater.*, 2018, **1**, 4218; (*d*) K. Sato, H. Masaki, M. Arayasu, Y. Oaki and H. Imai, *ChemPlusChem*, 2017, **82**, 177.

22 (*a*) R. Muramatsu, Y. Oaki, K. Kuwabara, K. Hayashi and H. Imai, *Chem. Commun.*, 2014, **50**, 11840; (*b*) K. Kuwabara, H. Masaki, H. Imai and Y. Oaki, *Nanoscale*, 2017, **9**, 7895.

23 K. Sato, M. Arayasu, H. Masaki, H. Imai and Y. Oaki, *Chem. Commun.*, 2017, **53**, 7329.

24 S. Yano, K. Sato, J. Suzuki, H. Imai and Y. Oaki, *Commun. Chem.*, 2019, **2**, 97.

25 (*a*) K. Sato, Y. Oaki and H. Imai, *Chem. Lett.*, 2016, **45**, 324; (*b*) K. Sato, Y. Oaki and H. Imai, *NPG Asia Mater.*, 2017, **9**, e377.

26 (*a*) F. Li, M. A. Winnik, A. Matvienko and A. Mandelis, *J. Mater. Chem.*, 2007, **17**, 4309; (*b*) K. M. Au, M. Chen, S. P. Armes and N. Zheng, *Chem. Commun.*, 2013, **49**, 10525; (*c*) M. Paven, H. Mayama, T. Sekido, H. J. Butt, Y. Nakamura and S. Fujii, *Adv. Funct. Mater.*, 2016, **26**, 3199; (*d*) H. Kawashima, M. Paven, H. Mayama, H. J. Butt, Y. Nakamura and S. Fujii, *ACS Appl. Mater. Interfaces*, 2017, **9**, 33351; (*e*) M. Takeuchi, H. Kawashima, H. Imai, S. Fujii and Y. Oaki, *J. Mater. Chem. C*, 2019, **7**, 4089.

27 K. Oyama, M. Seike, K. Mitamura, S. Watase, T. Suzuki, T. Omura, H. Minami, T. Hirai, Y. Nakamura and S. Fujii, *Langmuir*, 2021, **37**, 4599.